Applied Catalysis B: Environmental 168-169 (2015) 42–50

Contents lists available at ScienceDirect

Applied Catalysis B: Environmental

journal homepage: www.elsevier.com/locate/apcatb

Synthesis, characterization, and catalytic evaluation of Co_3O_4/γ-Al_2O_3 as methane combustion catalysts: Significance of Co species and the redox cycle

Qing Wang[a,b], Yue Peng[c], Jie Fu[c,*], George Z. Kyzas[d], Shah M. Reduwan Billah[e], Shuqing An[a,b,**]

[a] School of Life Science and Institute of Wetland Ecology, Nanjing University, Nanjing 210093, China
[b] Nanjing University Ecology Research Institute of Changshu (NJUecoRICH), Changshu 215500, Jiangsu, China
[c] School of Civil and Environmental Engineering, Georgia Institute of Technology, Atlanta, GA 30332, USA
[d] Laboratory of General & Inorganic Chemical Technology, Department of Chemistry, Aristotle University of Thessaloniki, Thessaloniki 54124, Greece
[e] Department of Chemistry, Durham University, South Road, Durham DH1 3LE, UK

ARTICLE INFO

Article history:
Received 28 July 2014
Received in revised form 9 December 2014
Accepted 11 December 2014
Available online 15 December 2014

Keywords:
Catalytic combustion of methane
Supported catalyst
Combustion synthesis
Cobalt species
Reducibility

ABSTRACT

A series of Co_3O_4/γ-Al_2O_3 catalysts with different Co_3O_4 loadings were prepared by incipient wetness impregnation (IWI) and a combination of IWI and subsequent combustion synthesis (CS), and tested for catalytic combustion of CH_4. The IWI/CS-*X* (*X* = 5, 10, 30 and 50, represented the Co_3O_4 loading as wt%) samples prepared via IWI/CS method exhibited higher catalytic activity than the IWI-*X* (*X* = 5, 10, 30 and 50) ones via IWI method. IWI/CS-30 showed the highest catalytic activity with T_{10} (10% CH_4 conversion) at 300 °C and T_{100} (complete conversion) at 550 °C. The structure characterization indicated the IWI/CS-*X* catalysts had a greater surface area with relatively lower Co_3O_4 crystallization and better Co_3O_4 dispersion compared with IWI-*X* samples. X-ray photoelectron spectroscopy (XPS) and UV–vis results revealed that surface $Co^{3+}/(Co^{2+} + Co^{3+})$ ratios of the IWI/CS-*X* samples was relatively higher than those of IWI-*X* ones. The surface Co^{3+} of the IWI/CS-*X* catalysts was easily reduced to Co^{2+} at 280–330 °C, whereas, only one difficult reduction process of Co_3O_4 to Co^0 was observed at 400–600 °C for all of the IWI-*X* samples according to hydrogen temperature-programmed reduction (H_2-TPR) results. Hence, the abundance of surface Co^{3+}, easy and fast redox cycle between Co^{2+} and Co^{3+} at low temperatures were the underlying mechanisms for the excellent catalytic performance of IWI/CS-*X* catalysts in CH_4 combustion.

1. Introduction

Increasing concern for the world's dependence on petroleum oil has generated great interest in the more efficient use of natural gas [1]. Compared to other fossil fuels, natural gas has the advantages of relatively abundant reserves, lower carbon intensity and higher fuel efficiency. Natural gas-powered vehicles emit 85% less NO_x, 70% less reactive hydrocarbons (HCs), and 70% less CO than similar gasoline-powered vehicles [2]. Nowadays, the compressed natural gas (CNG) engines are widely applied to vehicles. However, the main component of natural gas is CH_4, which is a more potent greenhouse gas than CO_2 with 72 times (over 20 years) the global warming potential (GWP) of CO_2 [3]. The emission of CH_4 from vehicles has become an important environmental issue and attracts more and more attentions [4,5]. Therefore, the after-treatment of unconverted CH_4 in vehicle exhausts has become imperative.

Due to the high stability of the CH_4 molecule and the low temperature of the exhausts of CNG vehicles (seldom exceeding 500 °C) [6], normal oxidation process is not effective to treat discharged CH_4. The catalytic combustion of CH_4 is believed to be a potential technology to oxidize CH_4 to CO_2 and H_2O at a relatively low temperature according to the literature references [7–12]. Noble metal-based catalysts, especially Pd-based ones, can exhibit outstanding catalytic properties [13,14]. However, the high cost limited their wide application. Considering the relatively abundant resources and lower cost, catalysts based on transition metal

* Corresponding author at: Daniel Lab 304, School of Civil and Environmental Engineering, Georgia Institute of Technology, Atlanta, GA 30332.
Tel.: +1 334 524 0068; fax: +1 334 524 0068.
** Corresponding author at: School of Life Sciences and Institute of Wetland Ecology, Nanjing University, Nanjing 210093, Jiangsu Province, China.
Tel.: +86 25 83594560; fax: +86 25 83594560.
E-mail addresses: jie.fu@ce.gatech.edu (J. Fu), anshq@nju.edu.cn (S. An).

http://dx.doi.org/10.1016/j.apcatb.2014.12.016
0926-3373/

oxides, such as Co, Cu, Cr, Mn, Fe and In oxides, are increasingly attractive [15,16]. Especially, Co_3O_4 displays excellent performance in catalytic combustion of CH_4 [17]. In order to maximize the surface area, and subsequently increase the reactivity, a catalyst is usually distributed over a support material. Xiao et al. [18] reported Al_2O_3 alone had the high activity for CH_4 combustion, over which the light-off temperature was only 500 °C. Al_2O_3 is a competitive candidate for preparation of supported Co catalysts with rich resources and relatively low cost. Unfortunately, the prepared Co_3O_4/Al_2O_3 catalyst showed low activity for CH_4 combustion due to poor dispersion of Co_3O_4 particles [18].

It is known that the preparation method has an important effect on the dispersion, specific surface area, morphology, and other structural and textural properties of metal-oxide catalysts, which influence their catalytic performances [19]. Incipient wetness impregnation (IWI) is a commonly used technique for the synthesis of heterogeneous catalysts. However, the main disadvantage of IWI is non-uniform deposition. The Co_3O_4/Al_2O_3 catalyst in Xiao et al.'s publication [18] was prepared by this conventional method and the active component, Co_3O_4, was not well dispersed on the support surface. During the last few decades, combustion synthesis (CS), a highly exothermic and self-sustaining reaction, has shown to be an efficient, quick, cost-effective and straightforward technique for producing a variety of high-surface area catalysts [20,21]. Recently, Zavyalova et al. has combined IWI and CS as a two-stage process to prepare heterogeneous catalysts, including transition-metal oxides on various supports [19,22]. They found that this method afforded Co_3O_4/γ-Al_2O_3 catalysts with a high dispersion of Co_3O_4 on the support, more structural defects and greater oxygen nonstoichiometry. However, the detailed comparative information on the structures of supported catalysts with different Co_3O_4 loadings prepared by this new method or the impregnation method is lacked.

The studies on the Co_3O_4/Al_2O_3 catalysts for CH_4 combustion are generally focused on the catalysts structure. However, the interaction between the Co species and the support is always ignored. The previous works [18,19] considered Co_3O_4 as an integrated particle and paid much attention on the dispersion of Co_3O_4. Actually, there exists Co^{2+} and Co^{3+} species in the Co particles and during the catalytic process Co^0 is also involved. Moreover, the oxidation reduction cycle between Co^{2+} and Co^{3+} is significant for the catalytic combustion of CH_4 [23]. However, the Co species as well as their redox cycle in the Co_3O_4/Al_2O_3 catalysts for CH_4 combustion have not been addressed.

In the present study, a series of Co_3O_4/γ-Al_2O_3 catalysts with different Co_3O_4 loadings were prepared by two methods, i.e., IWI alone and a combination of IWI and CS. The structure of the synthesized catalysts was characterized by a variety of methods (e.g., X-ray diffraction, Raman spectra, X-ray photoelectron spectroscopy, etc.) and their redox ability was evaluated by hydrogen temperature-programmed reduction. The catalytic capacity of Co_3O_4/γ-Al_2O_3 for catalytic combustion of CH_4 was studied within the test temperature range of 300–750 °C. The specific objectives were to: (1) evaluate the effects of two prepared methods (i.e., IWI and IWI/CS) and Co_3O_4 loadings on the catalysts products, and (2) disclose the roles of Co species and their redox cycle for the catalytic activity of the catalysts in CH_4 combustion.

2. Experimental

2.1. Catalyst preparation

For the IWI method, a required amount of aqueous $Co(NO_3)_2{\cdot}6H_2O$ solution was dripped onto γ-Al_2O_3. The mixture was stirred for 8 h, and the water was subsequently evaporated slowly at 90 °C. The obtained paste was dried overnight at 110 °C and then calcined at 700 °C for 4 h in static air. For the IWI/CS method, Co was introduced through the impregnation of γ-Al_2O_3 with aqueous solutions of $Co(NO_3)_2{\cdot}6H_2O$ and $(NH_2)_2CO$ (molar ratio = 2:1) [24]. The impregnated precipitates were dried at 110 °C and then placed in a crucible. A RCT basic hot plate (IKA WORKS, Wilmington, NC, USA) was used to initiate the exothermic reactions at the temperature of 230–250 °C for 5 min. After initiation, the self-propagating flameless combustion front in air was observed from the point of ignition and resulted in complete catalyst formation within 1–15 min. Catalysts prepared by IWI and IWI/CS were named as IWI-*X* and IWI/CS-*X*, respectively, where *X* (=5, 10, 30 and 50) represented the Co_3O_4 loading (wt%).

2.2. Catalyst characterization

The BET surface area was analyzed with a Nova Automated Gas Sorption System (Quantachrome Corporation, Boynton Beach, FL, USA) by measuring the N_2 adsorption isotherms at the liquid N_2 temperature (−196 °C). The pore size distribution was calculated according to the Barrett–Joyner–Halenda (BJH) method. The X-ray diffraction (XRD) measurements were performed on a D/max-2500 X-ray diffractometer (Rigaku Corporation, Tokyo, Japan) using Ni-filtered Cu Kα radiation. The inductively coupled plasma optical emission spectrometry (ICP-OES) measurements were carried out on an IRIS Intrepid II XSP ICP-OES instrument (Thermo Fisher Scientific, Waltham, MA, USA). The plasma power was 1150 W. The atomization gas pressure was 26.0 PSI, and the peristaltic pump rotation rate was 100 r/min. Transmission electron microscopy (TEM) images were taken on a JEM-2011 LaB6 instrument (JEOL, Tokyo, Japan). Raman spectra of the samples were recorded on a RM2000 Raman spectrophotometer (Renishaw plc, Wotton-under-Edge, Gloucestershire, UK). A 514.5 nm Ar^+ laser source operated at 4.7 mW was used, and samples were scanned over the wavelength range of 150–900 nm. X-ray photoelectron spectroscopy (XPS) data were obtained with an ESCALab220i-XL electron spectrometer (Thermo VG Scientific, East Grinstead, West Sussex, England) using 300 W Mg Kα radiation. The base pressure was approximately 3×10^{-9} mbar. The binding energies were referenced to the C 1s line at 284.8 eV from adventitious carbon. UV–vis diffuse reflectance spectra (UV–vis DRS) were recorded in air in the wavelength range 200–800 nm on a UV-2450 UV–vis spectrophotometer (Shimadzu Corporation, Kyoto, Japan). Hydrogen temperature-programmed reduction (H_2-TPR) experiments were performed on a Chemisorb 2720 instrument (Micromeritics Instrument Corporation, Norcross, GA, USA). In each experiment, 50 mg of catalyst was used and was pretreated in N_2 (50 mL/min) at 300 °C for 1 h before the test. TPR started at 100 °C, and the temperature was increased at a rate of 10 °C/min.

2.3. Catalytic activity measurements

The catalytic activities for CH_4 combustion were tested in a fixed-bed quartz reactor (i.d. 8 mm) with 250 mg of catalyst (40–60 mesh). The operating conditions were as follows: 0.2 vol% CH_4, 10 vol% O_2, and N_2 as the balance gas, with a total flow rate of 150 mL/min, which corresponds to a GHSV of approximately 36 000 mL/h g. The concentrations of CH_4 in the inlet and outlet gases were measured using an on-line 7890A gas chromatograph (Agilent Technologies, Santa Clara, CA, USA) within the test temperature range of 300–750 °C. In order to test the stability of catalysts, the catalytic reaction was continuously carried out at 800 °C for 10 days using IWI/CS-30. The CH_4 conversion gradually decreased (Fig. S1), indicating Co_3O_4/γ-Al_2O_3 catalysts were not stable at high temperature.

2.4. Principal components analysis

Principal components analysis (PCA) was carried out to study the relations between catalytic activity and physicochemical properties using SPSS13.0 for Windows (IBM Corporation, Armonk, NY, USA). The Kaiser-Meyer-Olkin (KMO) and Bartlett's test were introduced to evaluate the validity of PCA, and a >0.5 of KMO and significant Bartlett's test were requisite before the PCA.

3. Results and discussion

3.1. Structural properties of catalysts

ICP-OES experiments were performed to detect the actual Co_3O_4 loadings of Co_3O_4/γ-Al_2O_3 catalysts and the results are listed in Table 1. For IWI-5, IWI-50 and IWI/CS-10, the actual Co_3O_4 loadings were slightly higher than the initial Co_3O_4 dose, while the final Co_3O_4 loadings of IWI-10, IWI-30, IWI/CS-5, IWI/CS-30 and IWI/CS-50 were lower than the initial Co_3O_4 addition.

The BET surface area, pore volume, and average pore diameter of the Co_3O_4/γ-Al_2O_3 catalysts are summarized in Table 1 and pore size distribution is shown Fig. 1. Because the BET surface area of γ-Al_2O_3 (169 m^2/g) was significantly greater than that of Co_3O_4, γ-Al_2O_3 is considered to be the main contributor to the BET surface area of the Co_3O_4/γ-Al_2O_3 catalysts [25]. If γ-Al_2O_3 is assumed to be the only contributor to the BET surface area and pore volume of the Co_3O_4/γ-Al_2O_3 catalysts, the BET surface areas and pore volumes can be calculated as the following equation:

$$V_{cal.} = V_{det.} \times (1 - \%Co_3O_4) \quad (1)$$

where $V_{cal.}$ and $V_{det.}$ are the calculated and determined values, respectively, and $\%Co_3O_4$ is the actual Co_3O_4 loading. As shown in Table 1, the measured BET surface area values were slightly lower than the calculated values, except for that of IWI/CS-30, as were the pore volumes, except for those of IWI-5 and IWI-10. These results indicated some pore blockage of γ-Al_2O_3 by Co_3O_4 clusters. However, the measured pore volumes of IWI-5 and IWI-10 were somewhat higher than the calculated values, which may be related to a change in the pore size distribution and to a decrease in the number of small pores. With respect to the pore size distribution, the Co_3O_4 loading resulted in a fraction of small pores being blocked and an increase in pore diameters from 11.6 to 13.3 nm for IWI-5, IWI-10, IWI-30, IWI-50 and IWI/CS-50 (Table 1, Fig. 1). In addition, the measured pore diameters of IWI/CS-5 and IWI/CS-10 were almost the same as that of γ-Al_2O_3, because the pore size distribution of these samples did not change significantly. Concerning the IWI/CS-30 catalyst, both the relatively high BET surface area (131 m^2/g) and the small pore diameter (8.9 nm) revealed that Co_3O_4 were well dispersed on the surface of the γ-Al_2O_3; this level of dispersion was believed to be responsible for its outstanding catalytic performance in CH_4 combustion as described below.

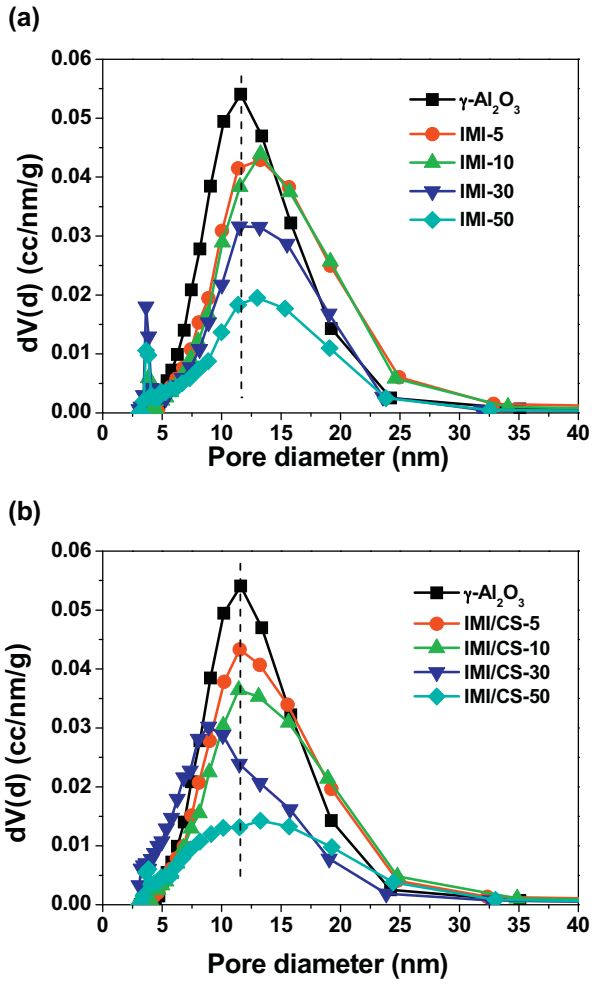

Fig. 1. Pore size distribution of γ-Al_2O_3 and Co_3O_4/γ-Al_2O_3 catalysts: (a) IWI-*X* catalysts, and (b) IWI/CS-*X* catalysts.

The XRD profiles of the Co_3O_4/γ-Al_2O_3 catalysts are presented in Fig. 2. For all of the catalysts, the only pure Co phase identified was the spinel-structured Co_3O_4 (JPCDS: 76-1802). The other observed diffraction peaks were attributed to γ-Al_2O_3. In the case of the IWI-*X* (*X* = 5, 10, 30 and 50) catalysts, increased Co_3O_4 loadings increased the intensity of the diffraction peaks of the spinel-structured Co_3O_4. IWI-50, in particular, showed diffraction peaks for only Co_3O_4 with no diffraction peaks that corresponded to the support. The diffraction peaks of Co_3O_4 in IWI/CS-*X* (*X* = 5, 10, 30 and 50) were broader and weaker than those of the IWI-*X* catalysts, which indicates the

Table 1
Actual Co_3O_4 loading, BET surface area, pore volume, pore diameter and Co_3O_4 crystallite size of Co_3O_4/γ-Al_2O_3 catalysts.

Catalysts	Actual Co_3O_4 loading (%)[a]	BET surface area (m^2/g)	Pore volume (ccg^{-1})	Pore diameter (nm)	Co_3O_4 crystallite size (nm)[c]
γ-Al_2O_3	–	169	0.53	11.6	–
IWI-5	5.1	149 (160[b])	0.53 (0.50)	13.3	14.9
IWI-10	9.4	143 (153)	0.51 (0.48)	13.3	17.1
IWI-30	28.4	116 (121)	0.37 (0.38)	13.3	20.9
IWI-50	50.2	77 (84)	0.25 (0.26)	13.3	30
IWI/CS-5	4.9	151 (161)	0.51 (0.51)	11.5	6.8
IWI/CS-10	10.4	135 (151)	0.46 (0.47)	11.4	9.4
IWI/CS-30	29.2	131 (120)	0.34 (0.38)	8.9	6.5
IWI/CS-50	46.8	73 (90)	0.24 (0.28)	13.3	10.7

[a] Calculated by Co content determined by ICP-OES.
[b] Calculated BET surface area or pore volume.
[c] Estimated by the Scherrer equation using the full-width at half-maximum of the characteristic diffraction peaks (indicated in Fig. 2).

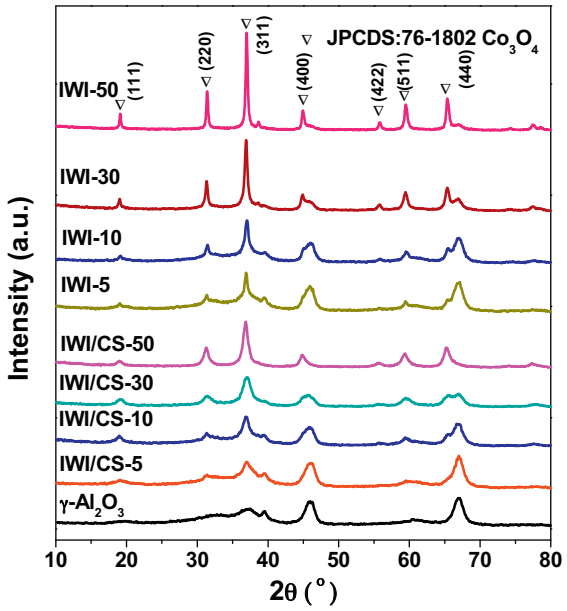

Fig. 2. XRD profiles of γ-Al_2O_3 and Co_3O_4/γ-Al_2O_3 catalysts.

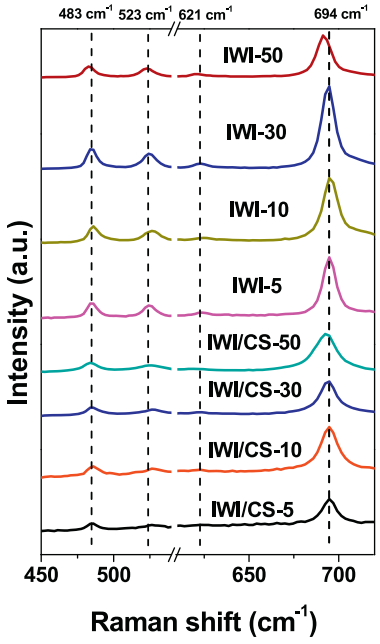

Fig. 3. Raman spectra of Co_3O_4/γ-Al_2O_3 catalysts.

lower degree of crystallization of Co_3O_4 and the higher degree of dispersion of Co_3O_4 in IWI/CS-*X* [19]. According to Scherrer equation, the Co_3O_4 crystalline size can be determined from each characteristic diffraction peak and the average values are summarized in Table 1. In general, the average Co_3O_4 crystallite size for all of the catalysts increased with increasing Co content because of the enhanced sintering and agglomeration of Co_3O_4 [26]. Specifically, the crystallite size of Co_3O_4 in the IWI-*X* samples increased from 14.9 to 30.0 nm as the Co_3O_4 loading increased from 5% to 50%. The crystallite sizes of IWI/CS-*X* catalysts were relatively smaller. The average crystallite size of IWI/CS-30 was the smallest (6.5 nm), which indicated the well-dispersion of Co_3O_4. When the Co_3O_4 loading was greater than 30%, the Co_3O_4 crystallite sizes of both IWI-*X* and IWI/CS-*X* catalysts rapidly increased, implying that the agglomeration of Co_3O_4 had occurred. The TEM pictures also showed IWI/CS-*X* catalysts had relatively smaller Co_3O_4 particles than IWI-*X* catalysts (Fig. S2).

Raman spectra of the Co_3O_4/γ-Al_2O_3 catalysts are shown in Fig. 3. Alumina itself is not Raman active, so all of the observed signals were caused by Co_3O_4 [18]. As shown in Fig. 3, the four peaks at 483, 523, 621, and 694 cm^{-1}, which correspond to the E_g, $F_{1g}{}^1$, $F_{2g}{}^1$, and $A_{1g}{}^1$ modes of the Co_3O_4 spinel structure, respectively, are observed for all of the samples, indicating that the surface layer of catalysts is covered by Co_3O_4 [27]. Systematic investigations of the effect of cations and isomorphous isotopic substitutions in spinels have shown that the 694 cm^{-1} vibration is the characteristic of the sublattice (octahedral/tetrahedral) in which the highest-valence cations are mainly located [28]. Any slight differences in this vibration can be associated with lattice distortion or residual stress of the spinel structure [29]. With increasing Co content, the $A_g{}^1$ vibration shifted slightly toward lower wavenumbers for both the IWI-*X* and IWI/CS-*X* samples. In addition, a slight increase in the full-width at half-maximum of the peak was also identified. All of these data indicated that with increasing Co content, the supported Co spinel catalysts exhibited a more defective structure. This effect could result in a higher concentration of Co in the low oxidation state and in a greater concentration of oxygen defects [30]. For the IWI/CS-*X* samples, the intensity of the Raman peaks did not significantly change with increased Co loading. Furthermore, the weaker and broader peaks for Co_3O_4 were detected in IWI/CS-*X* samples compared with those of IWI-*X* catalysts revealed that Co species were well dispersed on the surface of the γ-Al_2O_3 support, which was in agreement with the pore size distribution and XRD results [31].

The results of the BET surface area, pore size distribution, XRD and Raman spectra indicated that the IWI/CS method provided Co_3O_4/γ-Al_2O_3 catalysts with a smaller average crystalline size, a lower degree of crystallization of Co_3O_4 and a higher degree of dispersion of Co_3O_4 than did the IWI method. Because the combustion process is completed in a very short time during the syntheses and large quantities of vapors (e.g., CO_2, H_2O, and NO_2) are rapidly released, the growth of spinel crystals is limited. As a consequence, nano-sized grains with a smaller crystallite size and a greater surface area (compared with those of samples prepared via the IWI method) were obtained [19].

3.2. Cobalt species and the redox ability of catalysts

The Co 2p spectra of the Co_3O_4/γ-Al_2O_3 samples are shown in Fig. 4. The binding energy (BE) values are consistent with the presence of both Co^{2+} and Co^{3+}. The relevant band positions of these species differ by 0.9 eV, with the Co^{2+} 2p band occurring at a higher BE because of covalency and final-state effects [32]. Nevertheless, a spectral feature that could differentiate between Co^{2+} and Co^{3+} was a satellite for Co^{2+} peaks, because photoemitted electrons interact with core vacancy and valence electrons of Co^{2+} but not with those of Co^{3+} [33]. In the spectra of all of the samples, both the Co $2p_{3/2}$ and Co $2p_{1/2}$ peaks contained a satellite peak at BEs approximately 6 eV higher, which indicated the presence of Co^{2+}.

As shown in Table 2, the ratio of the intensity of the Co $2p_{3/2}$ satellite to that of the relevant main peak, I_{sat}/I_{main}, was used to indicate the surface $Co^{2+}/(Co^{2+}+Co^{3+})$ ratio. For the IWI/CS-*X* (*X* = 5, 10 and 30) samples, I_{sat}/I_{main} decreased from 0.6 to 0.4 as the Co_3O_4 loading was increased from 5 to 30 wt%, indicating an increase of Co^{3+} percentage in the catalyst surface. As the Co_3O_4 loading was increased, the spin–orbit separation between Co $2p_{3/2}$ and Co $2p_{1/2}$, $\Delta_{1/2-3/2}$, decreased from 15.4 to 15.1 eV (Table 2), which confirmed a parallel increase in the amount of surface Co^{3+}. However, the I_{sat}/I_{main} (0.7) of the IWI/CS-50 catalyst was greater than that of IWI/CS-5, which illustrated that excessive Co_3O_4 loading decreased the surface $Co^{3+}/(Co^{2+}+Co^{3+})$ ratio.

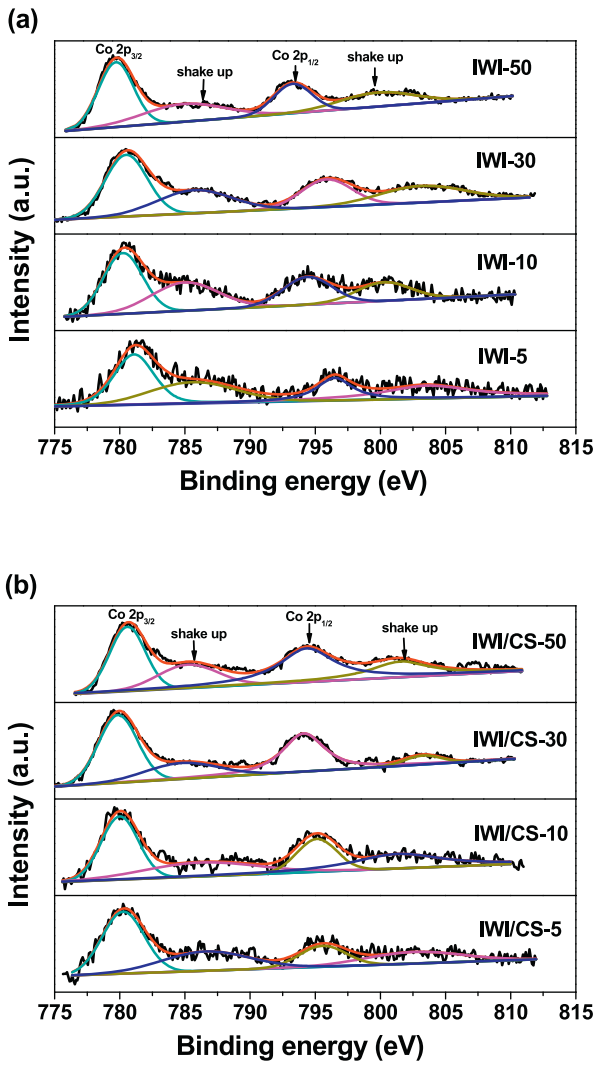

Fig. 4. Co2p spectra of Co_3O_4/γ-Al_2O_3 catalysts: (a) IWI-*X* catalysts, and (b) IWI/CS-*X* catalysts.

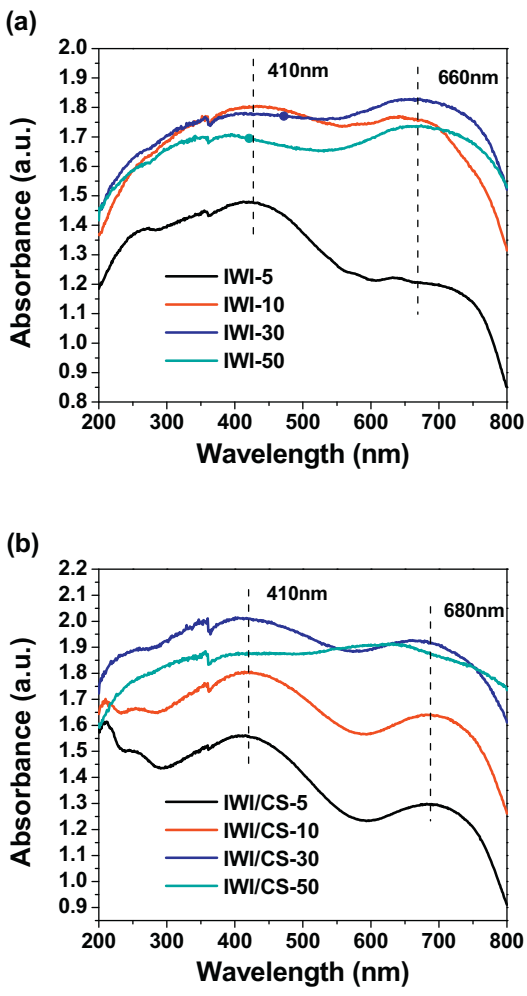

Fig. 5. UV–vis spectra of Co_3O_4/γ-Al_2O_3 catalysts: (a) IWI-*X* catalysts, and (b) IWI/CS-*X* catalysts.

The I_{sat}/I_{main} of the IWI-*X* (*X* = 10, 30 and 50) samples decreased from 0.9 (IWI-10), which was close to the value for CoO, to 0.8 (IWI-50) with increasing the Co_3O_4 loading from 10 to 50 wt%; this decrease indicated a slight increase in the amount of surface Co^{3+} [33]. Similarly, as the Co content was increased, $\Delta_{1/2-3/2}$ decreased from 16.3 (IWI-10) to 15.3 eV (IWI-50), and the BE of Co $2p_{3/2}$ shifted from 781.8 to 780.3 eV. These changes demonstrated an increase in surface Co^{3+}. However, the I_{sat}/I_{main} of the IWI-5 sample (0.7) was close to that of IWI/CS-5 (0.6), indicating a similar surface structure with a low Co_3O_4 loading between IWI-*X* and IWI/CS-*X* catalysts. It was clear that the IWI/CS-*X* samples tended to contain greater surface $Co^{3+}/(Co^{2+} + Co^{3+})$ ratios than did the IWI-*X* catalysts.

The UV–vis spectra of the Co_3O_4/γ-Al_2O_3 are shown in Fig. 5. For the IWI/CS-*X* samples (*X* = 5, 10 and 30), the intensities of the 410 nm absorption band, which was assigned to the octahedral Co^{3+} ($^1A_{1g} \rightarrow {}^1T_{2g}$) transition, and the 680 nm absorption band, which was assigned to the octahedral Co^{3+} ($^1A_{1g} \rightarrow {}^1T_{1g}$), increased pro-

Table 2
XPS parameters of Co_3O_4/γ-Al_2O_3 catalysts.

Sample	Co $2p_{3/2}$ main BE (eV)	Co $2p_{1/2}$ satellite BE (eV)	I_{sat}/I_{main} [a]	$\Delta_{1/2-3/2}$ [b] (eV)
IWI-5	781.1	785.8	0.7	15.7
IWI-10	780.8	785.8	0.9	16.3
IWI-30	780.4	784.8	0.8	15.8
IWI-50	780.3	785.7	0.8	15.3
IWI/CS-5	780.3	786.5	0.6	15.4
IWI/CS-10	780.0	785.6	0.5	15.2
IWI/CS-30	780.2	785.4	0.4	15.1
IWI/CS-50	780.8	786.4	0.7	15.8
CoO [33]	–	–	0.9	15.9
Co_3O_4 [33]	–	–	/[c]	15.0

[a] The I_{sat}/I_{main} was determined to ±0.1.
[b] Spin–orbit separation between the two main Co $2p_{3/2}$ and Co $2p_{1/2}$ peaks.
[c] Broad and low-intensity Co $2p_{3/2}$; the I_{sat}/I_{main} was not assessed in Ref. [33].

portionally with the Co content, which confirmed the presence of surface Co^{3+} on the catalysts [26]. The IWI/CS-50 sample exhibited two small absorption bands at 410 and 638 nm. The strong absorption at 638 nm may have been the combination of the 670 nm peak of Co_3O_4 and the 625 nm peak of tetrahedral Co^{2+} [34]. It has been suggested that surface Co^{2+} species were stabilized by strong interactions with the alumina and that this stabilization led to a decreased $Co^{3+}/(Co^{2+}+Co^{3+})$ ratio and was responsible for the negative impact on the catalytic activity [35]. For the IWI/CS-5 and IWI/CS-10 catalysts, the absorptions at 255 nm, which were observed when the Co_3O_4 loading was low, were due to the residual NO_3^- $n \rightarrow \pi^*$ charge-transfer band [36].

The spectrum of the IWI-5 sample was similar to that of IWI/CS-5, with two absorption peaks at 410 and 680 nm; the occurrence of these peaks indicated the presence of octahedral Co^{3+}. However, the poor catalytic performance of the IWI-5 sample was due to the difficult reduction of the surface Co^{3+}. The IWI-10, IWI-30 and IWI-50 samples all exhibited two peaks with almost the same intensity: one at 380–420 nm attributed to octahedral Co^{3+} and the other at 660 nm due to the combination of the 680 nm peak of Co_3O_4 and the 625 nm peak of tetrahedral Co^{2+} [37]. The intense absorption peaks at approximately 660 nm indicated the presence of abundant surface Co^{2+} for IWI-10, IWI-30 and IWI-50, which led to the decrease of $Co^{3+}/(Co^{2+}+Co^{3+})$ ratio.

To investigate the reducibility of the Co species in the Co_3O_4/γ-Al_2O_3 catalysts, H_2-TPR was performed. As is evident from the results in Fig. 6, the H_2-TPR profiles of the IWI-5 and IWI-10 catalysts exhibited only one reduction peak centered at 500 °C, whereas the profiles of both IWI-30 and IWI-50 exhibited three reduction peaks between 300 and 600 °C. The relative H_2 consumption increased with the increases of Co loadings (Table S1). To obtain detailed information about the reduction process, IWI-10 was characterized by XRD after reduction at 500 °C for 30 min under a 10% H_2/He atmosphere. Similarly, IWI-30 was analyzed by XRD after being reduced at 375, 480 and 550 °C, respectively. According to the results shown in Figs. 7 and 8, the reduction peaks at 512 and 500 °C for IWI-5 and IWI-10, respectively, could be assigned to the reduction of Co_3O_4 to Co^0. For the reduction peaks of IWI-30 and IWI-50, the first (weak) peak was attributed to the reduction process of some surface-adsorbed oxygen, whereas the second and third peaks were attributed to the direct reduction of Co_3O_4 to Co^0. Generally, Co_3O_4 will be reduced to CoO firstly. However, no apparent related reduction peaks were detected by XRD, indicating the reduction from Co_3O_4 to CoO in IWI-*X* samples was difficult.

The H_2-TPR profiles indicated 2 reduction peaks detected in IWI/CS-*X* samples (Fig. 6b). The relative H_2 consumption increased with increasing the Co loadings from 5% to 30%, and showed a decline trend when continuously increasing the Co loading to 50% (Table S1). With respect to the reduction of IWI/CS-30, Fig. 9 shows that after the catalyst was reduced at 300 °C and 670 °C for 30 min under a 10% H_2/He atmosphere, only the diffraction peaks for CoO, Co^0 and Al_2O_3 were observed. Therefore, for all of the IWI/CS-*X* samples, the first reduction peak between 280 and 330 °C was assigned to the reduction of Co_3O_4 to CoO, and the second broad reduction peak from 510 to 690 °C was attributed to the reduction of Co^{2+} to Co^0. The reduction peaks at low temperatures (280–330 °C) for the IWI/CS-*X* samples, due to the reduction of Co^{3+} to Co^{2+}, are thought to be highly relevant to the catalytic activity toward CH_4 combustion. The catalytic activity of IWI/CS-50 was between those of the IWI/CS-10 and IWI/CS-30 samples (as discussed below). Although the IWI/CS-50 catalyst contained a high Co_3O_4 loading, the BET surface area was 73 m^2/g and the Co_3O_4 crystallites were as large as 10.7 nm. In addition, the reduction of larger particles of Co_3O_4 on IWI/CS-50 was more difficult than the reduction of smaller particles, as evidenced by the H_2-TPR data (Fig. 6). This behavior was not consistent with the conclusions drawn by Solsona et al. [37]. Therefore, we inferred that the reduction of Co species is complex and is affected by numerous factors, including the content, the particle size and interactions between the support and the Co species. The effects of the particle size and the support interaction can be superimposed on each other. Whereas a decrease in the particle size of the metal oxide can result in a faster reduction rate due to a greater surface area/volume ratio, smaller particles may interact more with the support and slow the reduction [35].

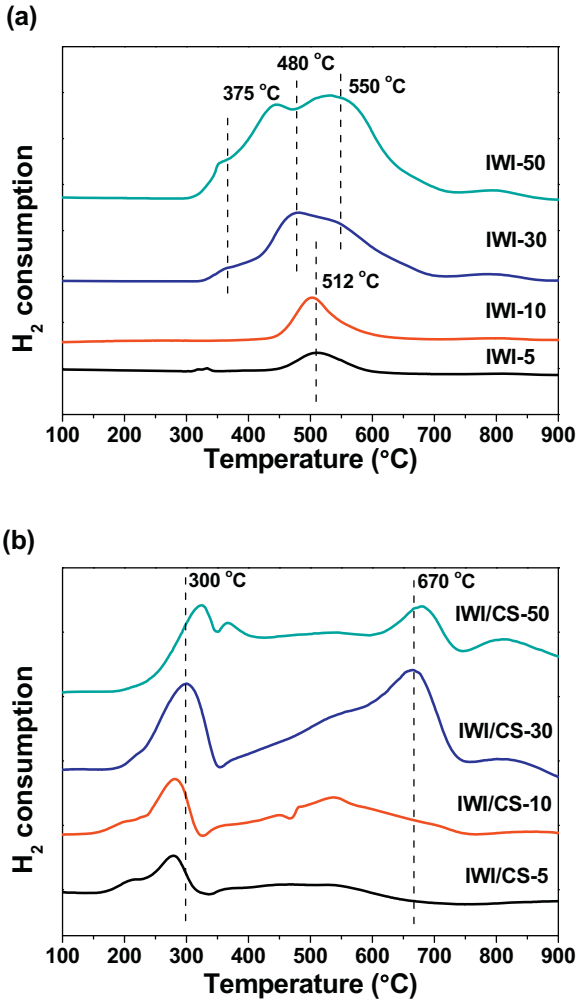

Fig. 6. H_2-TPR profile of Co_3O_4/γ-Al_2O_3 catalysts: (a) IWI-*X* catalysts, and (b) IWI/CS-*X* catalysts.

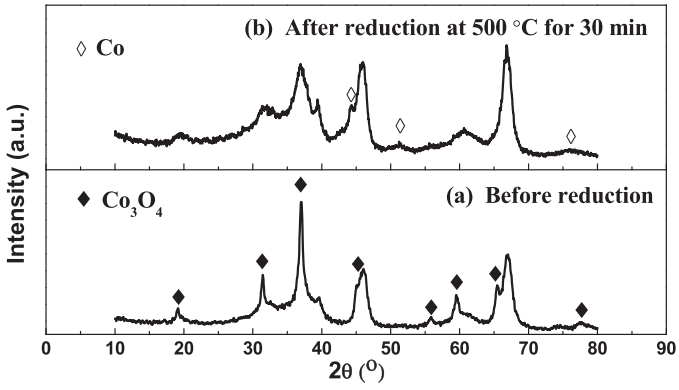

Fig. 7. XRD patterns of IWI-10 before and after reduction: (a) before reduction and (b) after reduction at 500 °C for 30 min under a 10% H_2/He atmosphere.

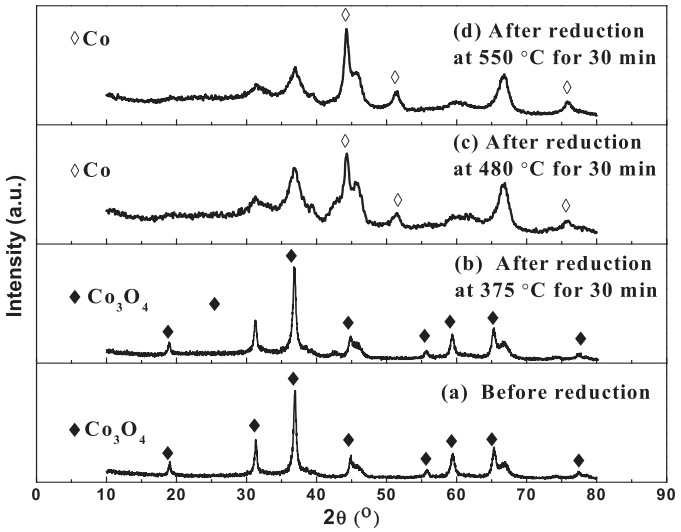

Fig. 8. XRD patterns of IWI-30 before and after reduction: (a) before reduction, (b) after reduction at 375 °C for 30 min under a 10% H_2/He atmosphere, (c) after reduction at 480 °C for 30 min under a 10% H_2/He atmosphere, and (d) after reduction at 550 °C for 30 min under a 10% H_2/He atmosphere.

The concentration of surface Co^{3+} on the IWI/CS-*X* samples was relatively high, and this surface Co^{3+} could be easily reduced to Co^{2+} at temperatures between 280 and 330 °C. Bahlawaue has demonstrated that the combustion of CH_4 follows a Mars–Van Krevelen mechanism, which involves two irreversible steps [23]. The CH_4 firstly reacts with the lattice oxygen resulting in its reduction and the formation of oxygen vacant site on the Co catalyst. The second step, which is rate-limiting, consists of the re-oxidation of the reduced catalyst site by the oxygen of the gas phase. The Mars–Van Krevelen mechanism indicates the importance of an effective electron sink, i.e., in terms of the reduction of Co^{3+} to Co^{2+} in the Co_3O_4 spinel structure, for harboring the excess electrons upon CO_2 formation, until being reoxidised by O_2 [38]. Ngamou and Bahlawane have reported that the higher reducibility of the edge-connected octahedrally coordinated Co^{3+} was responsible for the superior activity of Co_3O_4 toward the deep oxidation of aromatic compounds [39]. Moreover, Shen has stated that the CO molecule interacts

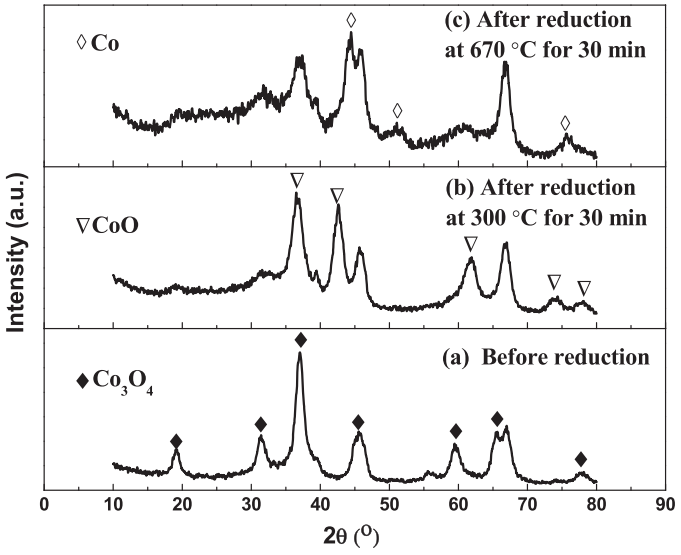

Fig. 9. XRD patterns of IWI/CS-30 before and after reduction: (a) before reduction, (b) after reduction at 300 °C for 30 min under a 10% H_2/He atmosphere, and (c) after reduction at 670 °C for 30 min under a 10% H_2/He atmosphere.

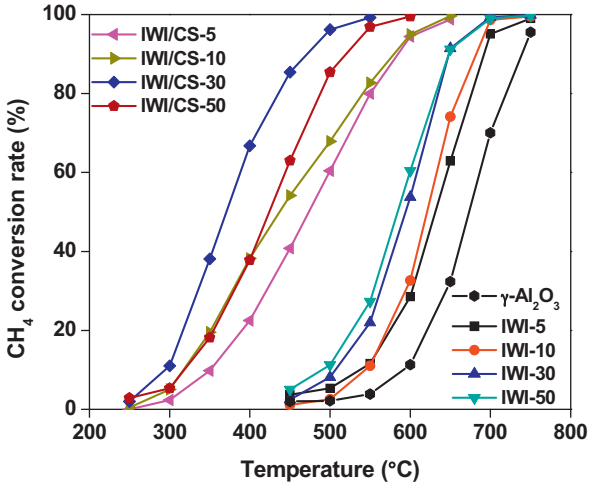

Fig. 10. Methane conversion over γ-Al_2O_3 and Co_3O_4/γ-Al_2O_3 catalysts. Reaction conditions: 0.2 vol.% CH_4, 10 vol.% O_2, and N_2 as the balance gas, with a total flow rate of 150 mL/min.

preferably with surface Co^{3+} cations, which is the only favorable site for CO adsorption, as confirmed both theoretically and experimentally [40]. These results strongly suggest that the existence of abundant and easily reduced surface Co^{3+} has a crucial effect on the catalytic combustion of CH_4. In addition, density functional theory (DFT) calculations of the Co_3O_4 (1 1 0) model illustrated that the bonding of O-3c with one Co^{2+} and two Co^{3+} cations was slightly more favorable than the bonding of O-2c with one Co^{2+} and one Co^{3+} cations, which provided further evidence for the key role of Co^{3+} in the catalytic combustion of CH_4.

The H_2-TPR, XPS and UV–vis results strongly indicated that the IWI/CS was a better method to prepare Co_3O_4/γ-Al_2O_3 catalysts, which created well-dispersed Co_3O_4 on the γ-Al_2O_3 support. The produced catalysts had high surface $Co^{3+}/(Co^{2+}+Co^{3+})$ ratios, and the surface Co^{3+} ions bound more favorably with O-3c. What is more, the prepared catalysts contained a greater amount of easily reduced Co species. Conversely, the catalysts prepared by the IWI method were poorly dispersed, contained Co species that were difficult to reduce from Co^{3+} to Co^{2+}, and exhibited low surface $Co^{3+}/(Co^{2+}+Co^{3+})$ ratios.

3.3. Catalytic combustion of methane

Fig. 10 shows the CH_4 conversion achieved at different temperatures on the catalysts with different Co_3O_4 loadings. The reaction products consisted entirely of CO_2 and H_2O in the temperature range investigated. For the IWI-*X* (*X* = 5, 10, 30 and 50) catalysts, the catalytic activity of CH_4 combustion increased with increasing Co_3O_4 loading, and IWI-50 exhibited the highest activity. The catalytic performances of IWI-30 and IWI-50 were nearly identical; these catalysts achieved 10% CH_4 conversion at approximately 500 °C and complete conversion at 700 °C. These results illustrate that the catalytic activity was exclusively due to the presence of Co_3O_4.

All of the catalysts prepared via the IWI/CS method showed better catalytic activity than the catalysts prepared via the IWI method. At the same reaction temperature, the reaction rate and turnover frequency (TOF) of IWI/CS-*X* catalysts were higher by more than one order of magnitude than IWI-*X* ones (Table S2, S3). When the Co_3O_4 loading was less than 30 wt%, the catalytic activity of IWI/CS-*X* catalysts quickly increased with increasing Co content. The IWI/CS-30 catalyst showed the highest activity, over which the T_{10} (10% CH_4 conversion) was 300 °C and the T_{100} (complete conversion)

occurred at 550 °C. The IWI/CS-50 catalyst showed an intermediate catalytic activity between those of the IWI/CS-10 and IWI/CS-30 samples.

The large discrepancy in the dispersion, degree of crystallization and reducibility of Co species between catalysts prepared via the IWI and IWI/CS methods resulted in different catalytic performance of CH_4 combustion.

For samples synthesized via the IWI method, the reduction of Co_3O_4 to Co^0 was the only reduction process of the cobalt species and this process was quite difficult (occurring at approximately 500 °C). Moreover, the re-oxidation of Co^0 to Co_3O_4 would also be difficult. Consequently, the difficult oxidation and reduction cycle between Co_3O_4 and Co^0 led to the lower activity of IWI-*X* catalysts toward CH_4 combustion. For the IWI/CS-*X* samples, the preparation process resulted in good dispersion of the Co species and the formation of abundant Co^{3+} on the surfaces of samples, which is easily reduced to Co^{2+} at approximately 300 °C. Hence, the easy and fast oxidation and reduction cycle between Co^{2+} and Co^{3+} at low temperatures was the main cause of the excellent catalytic performance of these catalysts in CH_4 combustion. In particular, for IWI/CS-30, the smallest average particle size (6.5 nm), the relatively higher BET surface area (131 m^2/g) and the highest surface $Co^{3+}/(Co^{2+}+Co^{3+})$ ratio played important roles in the outstanding catalytic properties of this catalyst. As a result, IWI/CS-30 exhibited the best catalytic methane combustion performance among the investigated samples. However, for IWI/CS-50, the excessive Co_3O_4 loading resulted in a diminished catalytic performance.

3.4. Relations between catalytic activity and physicochemical properties

The above results indicated the different catalytic activities of catalysts were resulted from the discrepancies of physicochemical properties including structural characteristics and Co species statuses. To comprehensively investigate the relations between catalytic activity and physicochemical properties, PCA was employed in the present study, which was proved an effective multivariate technique to interpret complex variations data [41–43].

For the convenient comparison of the catalytic activity, half CH_4 conversion temperature (CT50) values were calculated by sigmoidal fitting the CH_4 conversion curve (Fig. 10). For the IWI-*X* (*X* = 5, 10, 30 and 50) catalysts, the CT50 were 631, 620, 593 and 584 °C, respectively, and for IWI/CS-*X* (*X* = 5, 10, 30 and 50) samples, the CT50 were 472, 440, 371 and 423 °C, respectively. The CT50 of IWI/CS-30 is comparable with the previously reported data for the CH_4 combustion over Co_3O_4/γ-Al_2O_3 (320–396 °C) [19]. The

Table 3
Rotated component matrix for catalytic activity and physicochemical properties of Co_3O_4/γ-Al_2O_3 catalysts.

Properties	Component		
	1	2	3
CT50	**0.859**[a]	0.320	−0.333
P1	0.176	**−0.970**	0.102
P2	−0.293	**0.924**	−0.223
P3	−0.040	**0.982**	−0.121
P4	**0.936**	−0.005	0.130
P5	**0.754**	−0.399	**−0.430**
P6	**0.657**	0.337	**0.463**
P7	−0.080	0.137	**0.881**
P8	**0.972**	0.025	−0.015
P9	**0.778**	0.356	0.233
Eigenvalue	4.288	3.277	1.433
% Of variance explained	42.878	32.772	14.327
% Of cumulative	42.878	75.650	89.978

[a] |PCA loadings| > 0.4 are shown in bold.

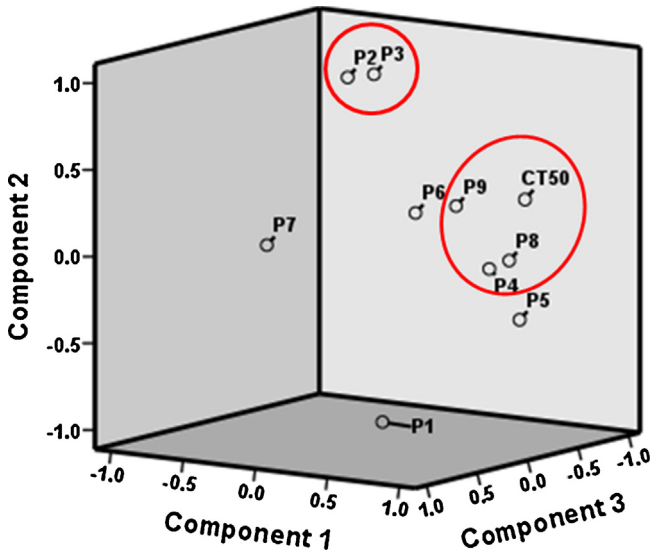

Fig. 11. Plot of loading of three principal components in PCA results. Symbols: CT50, half CH_4 conversion temperature; P1, Co_3O_4 loading; P2, BET surface area; P3, pore volume; P4, pore diameter; P5, Co_3O_4 crystallite size; P6, Co $2p_{3/2}$ main BE; P7, Co $2p_{1/2}$ satellite BE; P8, I_{sat}/I_{main}; P9, $\Delta_{1/2-3/2}$.

studied physicochemical properties included Co_3O_4 loading (P1), BET surface area (P2), pore volume (P3), pore diameter (P4), Co_3O_4 crystallite size (P5), Co $2p_{3/2}$ main BE (P6), Co $2p_{1/2}$ satellite BE (P7), I_{sat}/I_{main} (P8) and $\Delta_{1/2-3/2}$ (P9) (Tables 1 and 2).

Table 3 shows the results of the factor loadings with a varimax rotation as well as the eigenvalues. Three eigenvalues are higher than one and the three components explain 90% of the total variance. The relations among catalytic activity and physicochemical properties based on the three principal components are illustrated in three-dimensional (3D) space (Fig. 11). P4, P8 and P9 are close to CT50, indicating a similar change pattern. The high correlations imply the pore diameter and Co^{3+} content are the strongest factors that affect the catalytic activity. Smaller pore diameter and higher Co^{3+} content result in higher catalytic activity. The close relation between P2 and P3 suggests that BET surface area is mostly influenced by pore volume.

4. Conclusions

A combination of incipient wetness impregnation (IWI) and subsequent combustion synthesis (CS) proved to be an effective method to prepare Co_3O_4/γ-Al_2O_3 catalysts. The catalysts synthesized via the IWI/CS method contained well-dispersed Co species and abundant Co^{3+}, which played a crucial role in the catalytic combustion of CH_4. Particularly, IWI/CS-30 showed the best catalytic performance, and the total conversion of CH_4 occurred at 550 °C. However, the concentration of surface Co^{3+} on the IWI-*X* catalysts were relatively low, and the Co^{3+} was difficult to reduce to Co^{2+}, which led to lower activity of these catalysts toward the combustion of CH_4.

Acknowledgments

This study is financially supported by the S0926-3373(14) 00790-5Program for International S&T Cooperation Program of China (011DFG33480) and S0926-3373(14) 00790-5National Basic Research Program of China (2008CB418004).

Appendix A. Supplementary data

Supplementary data associated with this article can be found, in the online version, at http://dx.doi.org/10.1016/j.apcatb.2014.12.016.

References

[1] A.T. Ashcroft, A.K. Cheetham, M.L.H. Green, P.D.F. Vernon, Nature 352 (1991) 225.
[2] P. Goyal, Sidhartha, Atoms. Environ. 37 (2003) 5423.
[3] J.H. Li, X. Liang, S.C. Xu, J.M. Hao, Appl. Catal. B 90 (2009) 307.
[4] E.K. Nam, T.E. Jensen, T.J. Wallington, Environ. Sci. Technol. 38 (2004) 2005.
[5] M.E. Popa, M.K. Vollmer, A. Jordan, W.A. Brand, S.L. Pathirana, M. Rothe, T. Rockmann, Atmos. Chem. Phys. 14 (2014) 2105.
[6] D. Fino, N. Russo, G. Saracco, V. Specchia, Prog. Solid State Chem. 35 (2007) 501.
[7] L. Hu, Q. Peng, Y. Li, J. Am. Chem. Soc. 130 (2008) 16136.
[8] L.F. Liotta, G. Di Carlo, G. Pantaleo, A.M. Venezia, G. Deganello, Appl. Catal. B 66 (2006) 217.
[9] F. Yin, S. Ji, P. Wu, F. Zhao, C. Li, J. Catal. 257 (2008) 108.
[10] I.E. Beck, V.I. Bukhtiyarov, I.Y. Pakharukov, V.I. Zaikovsky, V.V. Kriventsov, V.N. Parmon, J. Catal. 268 (2009) 60.
[11] W. Tang, Z. Hu, M. Wang, G.D. Stucky, H. Metiu, E.W. McFarland, J. Catal. 273 (2010) 125.
[12] V.Y. Bychkov, Y.P. Tyulenin, M.M. Slinko, D.P. Shashkin, V.N. Korchak, J. Catal. 267 (2009) 181.
[13] K. Fujimoto, F.H. Ribeiro, M. Avalos-Borja, E. Iglesia, J. Catal. 179 (1998) 431.
[14] R.J. Farrauto, J.K. Lampert, M.C. Hobson, E.M. Waterman, Appl. Catal. B 6 (1995) 263.
[15] V.R. Choudhary, S. Banerjee, A.M. Rajput, Appl. Catal. A 234 (2002) 259.
[16] J.J. Spivey, Ind. Eng. Chem. Res. 26 (1987) 2165.
[17] M.F.M. Zwinkels, S.G. Jaras, P.G. Menon, T.A. Griffin, Catal. Rev. 35 (1993) 319.
[18] T.C. Xiao, S.F. Ji, H.T. Wang, K.S. Coleman, M.L.H. Green, J. Mol. Catal. A 175 (2001) 111.
[19] U. Zavyalova, P. Scholz, B. Ondruschka, Appl. Catal. A 323 (2007) 226.
[20] G. Avgouropoulos, T. Ioannides, H. Matralis, Appl. Catal. B 56 (2005) 87.
[21] P. Palmisano, N. Russo, P. Fino, D. Fino, C. Badini, Appl. Catal. B 69 (2006) 85.
[22] U.F. Zav'yalova, V.F. Tret'yakov, T.N. Burdeinaya, V.V. Lunin, N.B. Shitova, N.D. Ryzhova, A.N. Shmakov, A.I. Nizovskii, P.G. Tsyrul'nikov, Kinet. Catal. 46 (2005) 752.
[23] N. Bahlawane, Appl. Catal. B 67 (2006) 168.
[24] J.C. Toniolo, A.S. Takimi, C.P. Bergmann, Mater. Res. Bull. 45 (2010) 672.
[25] G. Jacobs, T.K. Das, Y.Q. Zhang, J.L. Li, G. Racoillet, B.H. Davis, Appl. Catal. A 233 (2002) 263.
[26] L.G.A. van de Water, G.L. Bezerner, J.A. Bergwerff, M. Versluijs-Helder, B.M. Weckhuysen, K.P. de Jong, J. Catal. 242 (2006) 287.
[27] W. Jia, M. Guo, Z. Zheng, T. Yu, E.G. Rodriguez, Y. Wang, Y. Lei, J. Electroanal. Chem. 625 (2009) 27.
[28] Q. Liu, L.C. Wang, M. Chen, Y. Cao, H.Y. He, K.N. Fan, J. Catal. 263 (2009) 104.
[29] I. Lopes, N. El Hassan, H. Guerba, G. Wallez, A. Davidson, Chem. Mater. 18 (2006) 5826.
[30] B. de Rivas, R. Lopez-Fonseca, C. Jimenez-Gonzalez, J.I. Gutierrez-Ortiz, J. Catal. 281 (2011) 88.
[31] P.G. Harrison, I.K. Ball, W. Daniell, P. Lukinskas, M. Cespedes, E.E. Miro, M.A. Ulla, Chem. Eng. J. 95 (2003) 47.
[32] D. Gazzoli, M. Occhiuzzi, A. Cimino, D. Cordischi, G. Minelli, F. Pinzari, J. Chem. Soc. Faraday Trans. 92 (1996) 4567.
[33] T.J. Chuang, C.R. Brundle, D.W. Rice, Surf. Sci. 59 (1976) 413.
[34] J.Y. Yan, M.C. Kung, W.M.H. Sachtler, H.H. Kung, J. Catal. 172 (1997) 178.
[35] B. Jongsomjit, J. Panpranot, J.G. Goodwin, J. Catal. 204 (2001) 98.
[36] U. Zavyalova, F. Girgsdies, O. Korup, R. Horn, R. Schlögl, J. Phys. Chem. C 113 (2009) 17493.
[37] B. Solsona, T.E. Davies, T. Garcia, I. Vazquez, A. Dejoz, S.H. Taylor, Appl. Catal. B 84 (2008) 176.
[38] P. Broqvist, I. Panas, H. Persson, J. Catal. 210 (2002) 198.
[39] P.H.T. Ngamou, N. Bahlawane, Chem. Mater. 22 (2010) 4158.
[40] X.W. Xie, Y. Li, Z.Q. Liu, M. Haruta, W.J. Shen, Nature 458 (2009) 746.
[41] J. Fu, C.P. Zhao, Y.P. Luo, C.S. Liu, G.Z. Kyzas, Y. Luo, D.Y. Zhao, S.Q. An, H.L. Zhu, J. Hazard. Mater. 270 (2014) 102.
[42] J. Fu, Q. Wang, H. Wang, H.X. Yu, X.W. Zhang, Environ. Sci. Pollut. Res. 21 (2014) 2898.
[43] J. Fu, S. Sheng, T. Wen, Z.M. Zhang, Q. Wang, Q.X. Hu, Q.S. Li, S.Q. An, H.L. Zhu, Ecotoxicology 20 (2011) 940.